People's Democratic Republic of Algeria
Ministry of Higher Education and Scientific Research
University M'Hamed BOUGARA – Boumerdes

Institute of Electrical and Electronic Engineering

Department of Power and Control

Final Year Project Report Presented in Partial Fulfilment of the Requirements for the Degree of

MASTER

In Electrical and Electronic Engineering

Option: **Control Engineering**

Option: **Power Engineering**

Title:

Direct Torque Control of Induction Motor Implementation Based FPGA Fed Three Level Inverter

Presented by:

BENCHEIKH Fares

DOUIB Lyamine

Supervisor:

Dr. METIDJI

Abstract

This thesis presents the implementation of Direct Torque Control (DTC) of induction machine utilizing FPGA to handle the issue of controlling the induction motor, since it is considered as one of the most difficult system to control because of its nonlinearity. Therefore, the direct torque control is principally a non-linear control in which the inverter switching states are imposed through a separate control of stator flux and electromagnetic torque of the motor. Furthermore, a Direct Torque Control (DTC) has become a popular technique for the control of induction motor drives as it provides fast dynamic torque response and robustness to machine parameter variations. Hysteresis band control is one of the simplest and most popular technique used in DTC of induction motor drives. Moreover, it is based on measuring the currents and voltages on the motor, and there are no mechanical sensors to estimate the instantaneous values of electromagnetic torque and stator flux. Afterward, they will be compared to the two adjustable references. And it is directly possible to reduce torque and flux errors by using inverter states.

Dedications

This thesis is dedicated to:

The sake of Allah, my Creator and my Master,

My great teacher and messenger, Mohammed (May Allah's peace and blesses be upon him), who taught us the purpose of life,

My parents, who never stop giving of themselves in countless ways,

My beloved brothers and sisters; particularly My beloved:

Tasnim, Wassim,

To all my family, the symbol of love and giving,

My friends who encourage and support me,

All the people in my life who touch my heart,

I dedicate this thesis

Fares.

The sake of Allah, my Creator and my Master,

My great teacher and messenger, Mohammed (May Allah bless and grant him)

Every challenging work needs self-efforts as well as guidance of Elders those who were very close to our heart.

My humble effort I dedicate to my sweet and loving

***Mother,** my beloved **father** and my **family members**,*

Whose affection, love, encouragement and prays of day and night make me able to get such success and honor.

*Along with all **my friends**, **hardworking** and respected*

Teachers.

Lyamine.

Acknowledgement

In the name of Allah, the Most Gracious and the Most Merciful
Alhamdulillah, all praises to Allah for the strengths and His blessing in completing this project.

We would like to express our deepest and sincere gratitude to our project Supervisor Dr. METIDJI Brahim,. It was a great privilege and honor to work and study under your supervision; we would like to thank the other teachers for their precious help during our work. Thank you very much.

Table of Contents

List of Figures

List of Tables

Table of variables

Variable	Description
U_a, U_b, Uc	Instantaneous values of the stator phase voltages
I_a, I_b, I_c	Instantaneous values of the stator phase currents
$\Psi A, \Psi B, \Psi C$	Flux linkages of the stator phase windings
α, β	Stator orthogonal coordinate system
$Us\alpha,\beta$	Stator voltages [V]
$^{i}s\alpha,\beta$	Stator currents [A]
$Ur\alpha,\beta$	Rotor voltages [V]
$ir\alpha,\beta$	Rotor currents [A]
$\Psi s\alpha,\beta$	Stator magnetic fluxes [Wb]
$\Psi r\alpha,\beta$	Rotor magnetic fluxes [Wb]
R_s	Stator phase resistance [Ohm]
R_r	Rotor phase resistance [Ohm]
L_s	Stator phase inductance [H]
P	Number of pole pairs
T_e	Electromagnetic torque [Nm]

List of Abbreviation

Abbreviation	Meaning
AC	Alternating Current
DC	Direct Current
DSP	Digital Signal Processor
DTC	Direct Torque Control
FPGA	Field Programmable Gate Array
FOC	Field Oriented Control
IM	Induction Motor
MOSFET	Metal Oxide Semiconductor Field Effect Transistor
NPC	Neutral Point Clamped
PI	Proportional-Integral
PWM	Pulse Width Modulation
SVM	Space Vector Modulation
VSI	Voltage Source Inverter
RTL	Register Transfer Level
FSM	Finite State Machine

1

INTRODUCTION

1.1 Motivation

The DTC method has become an attraction to many researchers for developing advanced motor control due to its simplicity and fast torque dynamic response. It also has gained widely acceptance in industrial.

In recent years, it can be noticed that the DTC technology has replaced gradually the Field Oriented Control (FOC) method in many electric drive applications. This mainly due to the fact that the DTC has simpler structure compared to the FOC that requires a current controller, frame transformer, speed sensor and knowledge of machine parameters. Without the requirement of speed sensor and knowledge of machine parameters, these make sense that the DTC is normally known as sensorless and robust control in controlling the flux as well as electromagnetic torque.

1.2 GENERAL INTRODUCTION

The cage rotor induction motor became of particular interest as it is robust, reliable and maintenance free. It has lower cost, weight and inertia compared to commutator DC motor of the same power rating. Furthermore, induction motors can work in dirty and explosive environments. However, the relative simplicity of the

latest control algorithms. Two most spread industrial control schemes employs vector or field-oriented control (FOC) and direct torque control (DTC).

DTC has a relatively simple control structure. The original DTC scheme was proposed by Takahashi in 1986 [1] and uses hysteresis controllers to control independently both the stator flux and the torque. It is also known that DTC drive is less sensitive to parameters de-tuning (only stator resistor is used to estimate the stator flux) and provides a high dynamic performance than the classical vector control.

This controller produces a variable switching frequency and consequently large torque and flux ripples and high currents distortion[2]. And since in practice the hysteresis controllers are digitally implemented. This means that they function within discrete time Ts. Consequently, the control of whether the torque or the flux is within the tolerance limits, often delays depending on the duration of the sampling period. Therefore, we can determine that the sampling frequency is the most important parameters to reduce those errors.

It is possible to reduce ripple by reducing the sampling period [3]. Moreover, the effectiveness in minimizing the output torque ripple can be achieved if only a high switching frequency is applied. Unfortunately, microcontrollers and DSPs are inadequate for the above requirement. For this reason, recent DTC drives have been implemented by using fast processing devices such as FPGAs [4]. FPGAs provide rapid prototyping, high performance signal processing, high precision and flexibility due to their reconfigurable architecture. FPGAs enable hard real time processing and high computing power based on a direct hardware implementation of algorithms and functionalities [5].

For that reason, our project will be aimed to implement the flux and torque estimations for hysteresis-based DTC utilizing FPGA using VHDL code. And as they involve complex calculations (e.g. integrals, square-root, multiplication and

precise current scaling factor). The VHDL code for each part of the whole design will be verified using the co-simulation interface between Matlab/Simulink and HDL simulators Modalism.

1.3 Thesis Organization

The thesis consists of five chapters. Chapter 1 is an introduction. In Chapter 2 mathematical model of IM with the two most used methods for controlling torque and flux, voltage source three-level inverter construction with space vector method. Chapter 3 the basic principles of direct torque control are presented. Those bases are common for classical DTC. Chapter 4 is devoted to analysis and synthesis of DTC control technique implementation using VHDL code with hardware design of three level inverter on PCB are presented, with experimental results discussion. Chapter 5 consists of general conclusion followed by the drawbacks of DTC and the future work.

2

State of Art

In this chapter is made a review of the most relevant concepts to the development of this thesis. The principal electric induction motors and the mathematical model and their control methods are compared. However, in this project the natural extension of classical DTC method will be the main subject of this thesis. Also, a survey of most common multi-level voltage source converters, and the Neutral Point Clamped will be used in this project.

2.1 Introduction

The induction motor is one of the most important AC machines used in industrial applications as often described as the ‘workhorse of industry because of its well-known advantages: good self-starting capability, simple construction, low cost, reliable and need less maintenance etc.

The three-phase induction machine (IM) is widely used in industrial applications, such as belt conveyors, pumps, fans, cranes, wind energy, electric vehicle etc.

It presents great mechanical sturdiness and there is a good standardization between IM manufacturers worldwide. Nevertheless, the relative simplicity of the operation of the motor hides a great complexity, especially when it is aimed at controlling the performed electromechanical conversion.

2.2 Construction and Principle Operation of Induction Motor

2.2.1 Construction of Induction Motors

Like most motors, an AC induction motor has a fixed outer portion, called the stator and a rotor that spins inside with a carefully engineered air gap between the two.

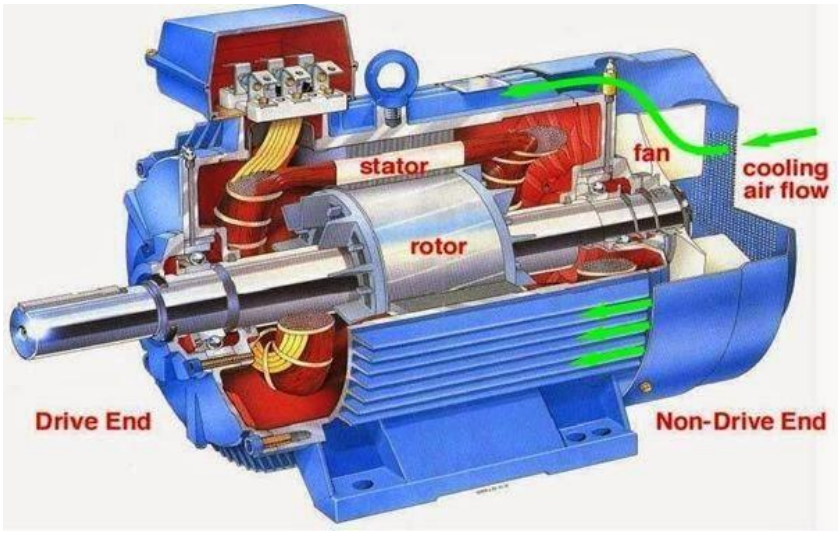

Figure 2.1Construction of Induction Motor

2.2.1.1 Stator

The stator is made up of several thin laminations of aluminum or cast iron. They are punched and clamped together to form a hollow cylinder (stator core) with slots as shown in Figure 2.2. Coils of insulated wires are inserted into these slots. Each grouping of coils, together with the core it surrounds, forms an electromagnet (a pair of poles) on the application of AC supply. The number of poles of an AC induction motor depends on the internal connection of the stator windings. The stator windings are connected directly to the power source. Internally they are connected in such a way, that on applying AC supply, a rotating magnetic field is created [6].

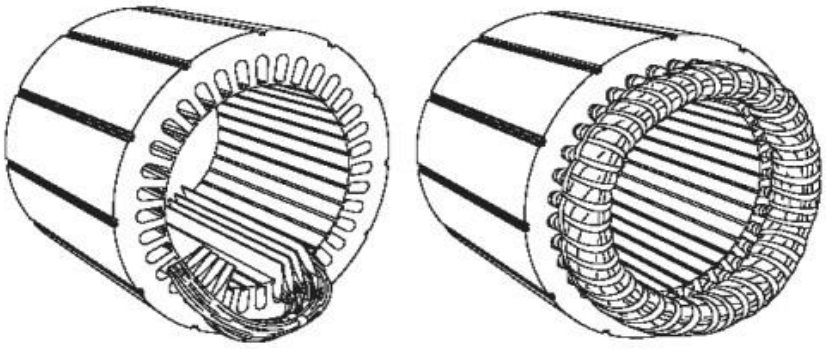

Figure 2.2 A Typical Stator[6]

2.2.1.2 Rotor

The rotor is made up of several thin steel laminations with evenly spaced bars, which are made up of aluminum or copper, along the periphery. In the most popular type of rotor (squirrel cage rotor), these bars are connected at ends mechanically and electrically by the use of rings. Almost 90% of induction motors have squirrel cage rotors. This is because the squirrel cage rotor has a simple and rugged construction. The rotor consists of a cylindrical laminated core with axially placed parallel slots for carrying the conductors. Each slot carries a copper, aluminum, or alloy bar. These rotor bars are permanently short-circuited at both ends by means of the end rings, as shown in Figure 2.3. This total assembly resembles the look of a squirrel cage, which gives the rotor its name [6].

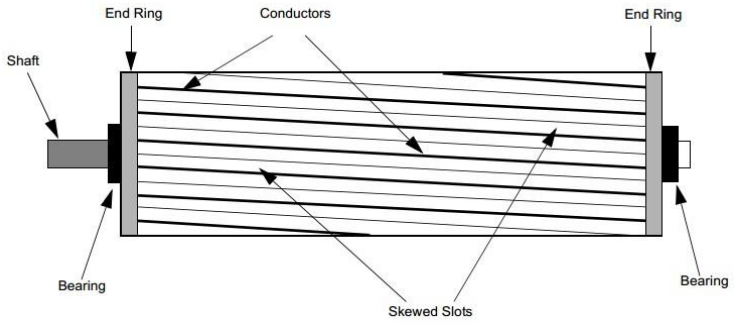

Figure 2.3: A typical squirrel cage rotor[6]

2.2.2 Principal of Operation

Virtually all electrical motors use magnetic field rotation to spin their rotors. A three-phase AC induction motor is the only type where the rotating magnetic field is created naturally in the stator because of the nature of the supply. DC motors depend either on mechanical or electronic commutation to create rotating magnetic fields. A single-phase AC induction motor depends on extra electrical components to produce this rotating magnetic field. Two sets of electromagnets are formed inside any motor. In an AC induction motor, one set of electromagnets is formed in the stator because of the AC supply connected to the stator windings. The alternating nature of the supply voltage induces an Electromagnetic Force (EMF) in the rotor (just like the voltage is induced in the transformer secondary) as per Lenz's law, thus generating another set of electromagnets, hence the name-induction motor Interaction between the magnetic field of these electromagnets generates twisting force, or torque. As result, the motor rotates in the direction of the resultant torque. [7]

2.3 Mathematical Model of Induction Motor

There are a number of ACIM models; the model used for vector control design can be obtained by using the space vector theory. The 3-phase motor quantities, such as currents, voltages, and magnetic fluxes, are expressed in terms of complex space

vectors. Such a model is valid for any instantaneous variation of voltage and current and adequately describes the performance of the machine under steady-state and transient operation. The motor is considered to be a 2-phase machine by using two orthogonal axes with this model, the number of equations is reduced and the control design is simplified [8].

When describing a three-phase IM by a system of equations, the following simplifying assumptions are made [8]:

- The three-phase motor is symmetrical.
- Only the fundamental harmonic is considered, while the higher harmonics of the spatial field distribution and of the magneto-motive force (MMF) in the air gap are disregarded.
- The spatially distributed stator and rotor windings are replaced by a specially formed, so called concentrated coil.
- The effects of anisotropy, magnetic saturation, iron losses, and eddy currents are neglected.
- The coil resistances and reactance are taken to be constant.
- in many cases, especially when considering steady state, the current and voltages are taken to be sinusoidal.

Taking into consideration the earlier-stated assumptions, the following equations of the instantaneous stator phase voltage values can be written as follows:

$$U_A = I_A R_s + \frac{d\Psi A}{dt} \tag{2.3.a}$$

$$U_B = I_B R_s + \frac{d\Psi B}{dt} \tag{2.3.b}$$

$$U_C = I_C.R_s + \frac{d\Psi C}{dt} \quad (2.3.c)$$

It is assumed that the three-phase system is balanced:

$U_{A0} + U_{B0} + U_{C0} = 0$

Under all the previous consideration the three equations can be presented in to The vector which is represented in a αβ-plane. This is a two-dimensional plane transformed from a three-dimensional plane containing the vectors of the three Phases as shown in following figure2.4.

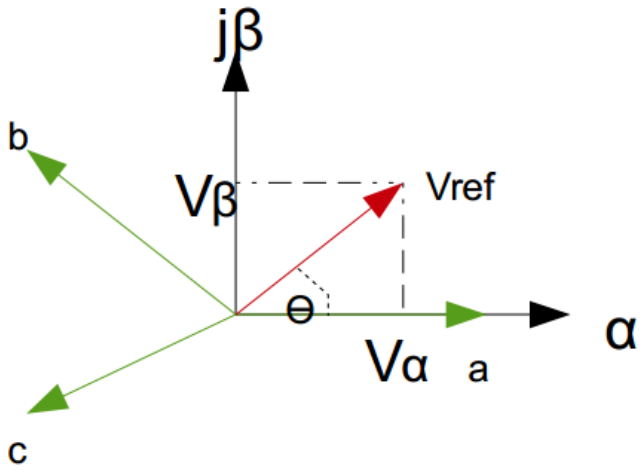

Figure 2.4 The reference vector in the two and three-dimensional plan

So, we ca write:

$$V_\alpha + jV_\beta = \frac{2}{3}(U_A + U_B e^{j2\pi/3} + U_C e^{-j2\pi/3}) \quad (2.4)$$

Using the space vector method, the IM model equation can be written as:

The stator voltage differential equations:

$$Us\alpha = I_{s\alpha}.R_s + \frac{d\Psi s\alpha}{dt} \quad (2.4.a)$$

$$Us\beta = I_{s\beta}.R_s + \frac{d\Psi s\beta}{dt} \quad (2.4.b)$$

The rotor voltage differential equations:

$$Ur\alpha = 0 = I_{r\alpha}.R_{sr} + \frac{d\Psi r\alpha}{dt} + \omega\Psi_{r\beta} \quad (2.4.c)$$

$$Ur\beta = 0 = I_{r\beta}.R_r + \frac{d\Psi r\beta}{dt} + \omega\Psi_{r\alpha} \quad (2.4.d)$$

The stator and rotor flux linkages expressed in terms of the stator and rotor current space vectors:

$$\Psi_{s\alpha} = L_s i_{s\alpha} + L_m i_{r\alpha} \quad (2.5.a)$$

$$\Psi_{s\beta} = L_s i_{s\beta} + L_m i_{r\beta} \quad (2.5.b)$$

$$\Psi_{r\alpha} = L_r i_{r\alpha} + L_m i_{s\alpha} \quad (2.5.c)$$

$$\Psi_{r\beta} = L_r i_{r\beta} + L_m i_{s\beta} \quad (2.5.d)$$

The electromagnetic torque can be expressed as a function of the stator flux and the current space as follows:

$$Te = \frac{3}{2}P(\Psi_{s\alpha} i_{s\beta} - \Psi_{s\beta} i_{s\alpha}) \quad (2.6)$$

2.4 **Control**

These features depend on the applied control strategy. The main goal of the chosen control method is to provide the best possible parameters of drive. Additionally, a very important requirement regarding control method is simplicity (simple algorithm,

simple tuning and operation with small controller dimension leads to low price of final product).

A general classification of the control techniques for the IM methods is made by Holtz from the point of view of the controlled signal [9]

1-Scalar control: These techniques are mainly implemented through direct measurement of the machine parameters.

2-Vector control: These techniques are realized both in analogue version (direct measurements) and digital version (estimation techniques).

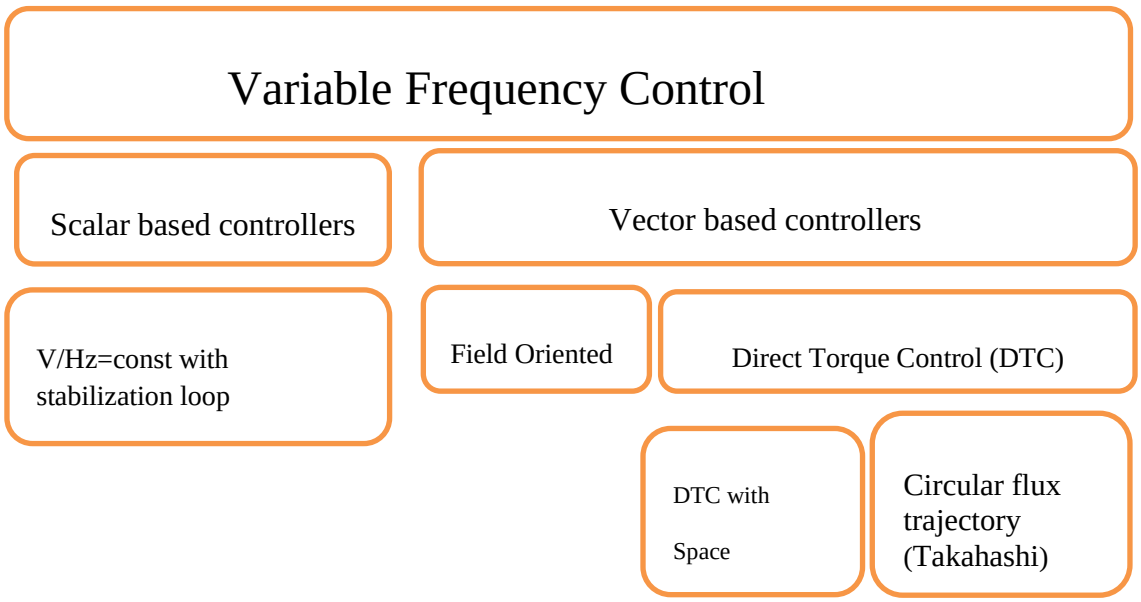

Figure 2.5 Holtz classification of control techniques

The scalar control is based on a relation valid for steady states, only the magnitude and frequency (angular speed) of voltage, currents, and flux linkage space vectors are controlled. Thus, the control system does not act on space vector position

during transient. Therefore, this control is dedicated for application, where high dynamics is not demanded.

In search of a simpler and more robust high-performance control system a new vector control called direct torque control (DTC) was developed. It allows direct control flux and torque quantities without inner current control loops. Using hysteresis controllers for flux and torque control loops made this control concept very fast and not complicated.

2.4.1 Field Oriented Control

Field oriented control method, known popularly as vector control is widely used in modern industrial systems. The field oriented control method of the motor is realized for current components in d-q rotating coordinate system [10].

In the field oriented control system, a stator current d-component adjusts the rotor flux in the motor, while the combination of d and q- components adjusts the motor torque. By applying the decoupling block in the particular d and q control parts the control of flux and torque can be done independently

2.4.2 Direct Torque Control

The field-oriented control is an attractive control method but it has a serious drawback: it relies heavily on precise knowledge of the motor parameters. The rotor time constant is particularly difficult to measure precisely, and to make matters worse it varies with temperature.

A more robust control method consists first in estimating the machine stator flux and electric torque in the stationary reference frame from terminal measurements.

The estimated stator flux and electric torque are then controlled directly by comparing them with their respective demanded values using hysteresis comparators.

The outputs of the two comparators are then used as input signals of an optimal switching table [11], [12].

2.5 Voltage Source Multilevel Inverters

Multi-level converters have been receiving attention in the recent years and have been proposed as the best choice in a wide variety of medium voltage (MV) applications [13]. They enable a commutation at substantially reduced voltages and an improved harmonic spectrum without a series connection of devices, which is the main advantage of a multi-level structure.

Other advantages of these topologies are better output voltage quality, reduced electromagnetic interference (EMI) problems, and lower overall losses in some cases. However, today they have a limited commercial impact due to their disadvantages such as high control complexity and increased power semiconductor count when comparing the 2L-VSC with the 3L-NPC VSC.

Multilevel inverter structures are becoming increasingly popular for high power applications, because their switched output voltage harmonics can be considerably reduced by using several voltage levels while still switching at the same frequency. As well, higher input DC voltages can be used since semiconductors are connected in series for multilevel inverter structures, and this reduces the DC voltage each device must withstand [14].

Among the high-power multi-level converters, three topologies have been successfully implemented as standard products for medium voltage industrial drives. The Neutral Point Clamped Voltage Source Converter (NPC VSC), the Flying Capacitor Voltage Source Converters (FLC VSC), and the Series Connected H-Bridge Voltage Source Converters (SCHB VSC). These topologies can be classified by the type their respective number of DC sources, as it is displayed in figure 2.6.

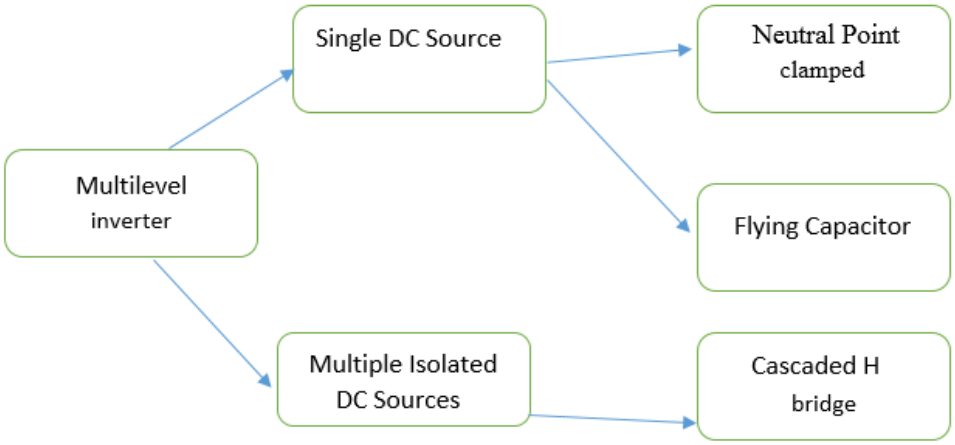

Figure 2.6 Classification of multi-level voltage source converters

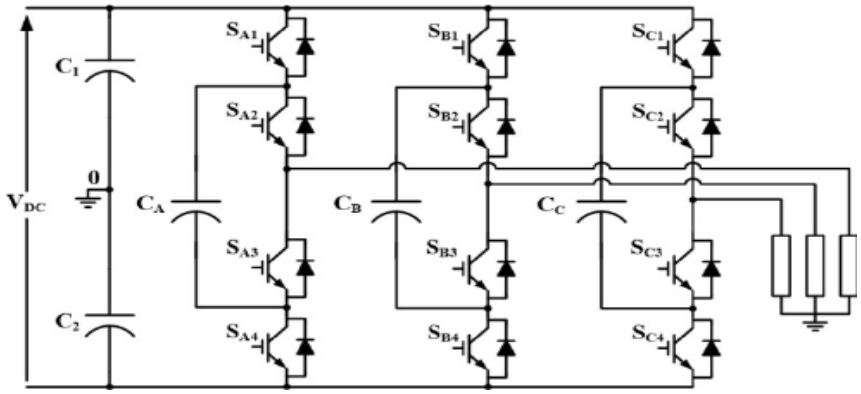

Figure 2.7 three level flying-capacitor inverter

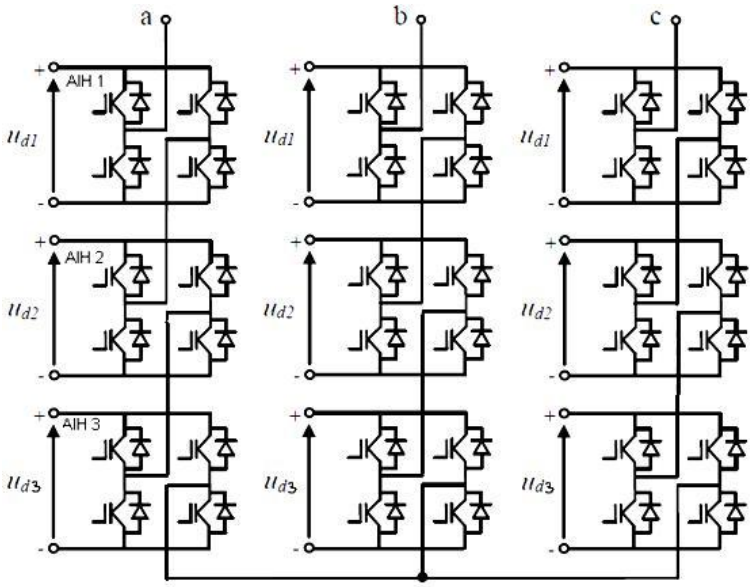

Figure 2.8 three-phase structure of a multilevel cascaded H-bridges.

2.6 NEUTRAL POINT CLAMPED INVERTER

The three-level neutral-point-clamped voltage source inverter (NPC VSI) was introduced by Nabae in 1981 [15] and is probably the most popular among the multilevel converter topologies for high voltage, high power applications. As shown in Figure 2.9, the NPC VSI is supplied by two series-connected capacitors (C1 and C2), where both capacitors are charged to an equal potential of V_{DC}, with the DC-link middle point 'o' as a zero DC voltage neutral point. Each phase leg of the NPC VSI consists of four series-connected switching devices and two clamping diodes. These diodes clamp the middle switches' potential to the DC-link point 'o'.

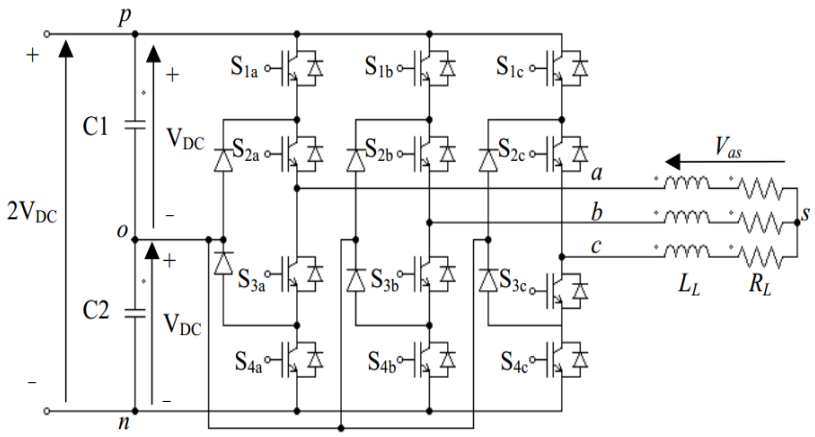

Figure 2.9 The schematic diagram of a conventional three-level neutral-point-clamped

In order to generate the three-level output, the switching devices in each phase leg are controlled according to the switching combinations presented in Table 2.1. At any time, only two of the four switching devices are turned on and the output terminal can be connected to any of the DC-link points (p, o or n), which can be represented by a switching state (P, O or N); for example, switching state P represents the connection of the output terminal to the DC-link point 'p'. Using the DC-link middle point 'o' as a reference, the NPC VSI is obviously able to generate three distinct voltage levels at the output terminal of each phase leg, V_{xo} which can be determined using the following equation

$$V_{XO} = (S_{1x} + S_{2x} - 1) * V_{dc} \quad (2.7)$$

Where S_{1x} and S_{2x} represent the tow above switches for each leg ($x \in \{a, b, c\}$) [16], and for S_{3x} S_{4x} are the inverse state of S_{1x} and S_{2x} respectively.

Table2.1 The switching combination for the switches in each phase leg of the three-level neutral-point-clamped voltage source inverter (x ∈{a, b, c})

S_{1x}	S_{2x}	V_{XO}	Switching state
ON	ON	Vdc	P
OFF	ON	0	O
OFF	OFF	-Vdc	N

These switching states are able to generate specific output phase (line-to-load neutral, s) using the following equations [16].

V_{as}= (2/3). V_{dc} (S_{1a} + S_{2a} -1/2. (S_{1b} +S_{2b} + S_{1c} + S_{2c}).

V_{bs}= (2/3). Vdc (S_{1b} + S_{2b} -1/2. (S_{1a} +S_{2a} + S_{1c} + S_{2c}).

Vcs= (2/3). Vdc (S_{1c} + S_{2c} -1/2. (S_{1b} +S_{2b} + S_{1c} + S_{2c}).

In order to generate a set of balanced and sinusoidal output waveforms, the concept of space vectors is used. the output phase voltages generated by the switching states of the NPC VSI have to be converted into space vectors using the following transformation:

$$V_\alpha + jV_\beta = \frac{2}{3}(V_{as} + V_{bs}e^{j2\pi/3} + V_{cs}e^{-j2\pi/3})$$

By doing all the switching state combinations the following output voltages can be deduced as shown in table 2.2.

Based on the voltage magnitudes, the voltage space vectors can be divided into four groups: zero voltage vector ZVV (V0), small voltage vectors SVV (V1, V4, V7, V10, V13 and V16), middle voltage vectors MVV (V3, V6, V9, V12 and V15) and

large voltage vectors LVV (V2, V5, V8, V11, V14 and V17). Figure 2.10 shows the space vector diagram of the NPC VSI that is formed by these voltage space vectors, where the ZVV and SVV obviously have redundant switching states that offer an additional degree of freedom in the synthesize of the output voltage vector.

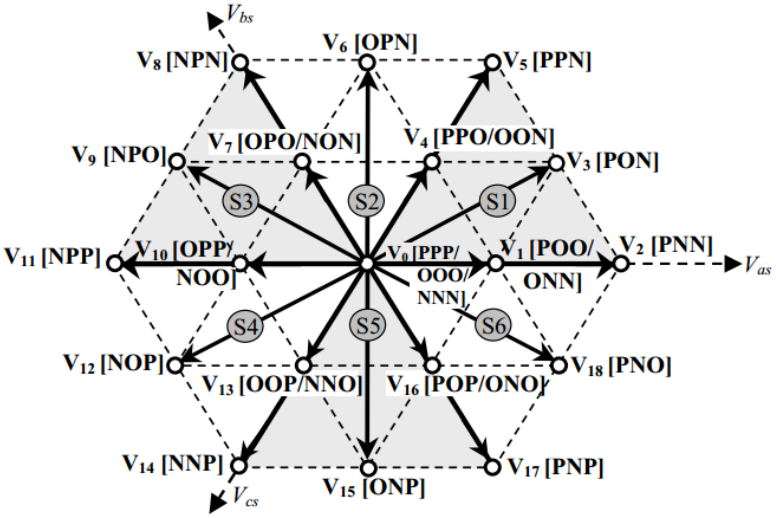

Figure 2.10 The space vector diagram for the three-level neutral-point-clamped voltage

Table 2.2 The magnitude and angle of each voltage space vector formed by the switching state of the NPC VSI using the space vector transformation.

Switching state combination			Output voltage vectors		
A	b	C	Vector	Magnitude	Angle
P	P	P			
O	O	O			
N	N	N	V_0	0V	0
P	O	O			
O	N	N	V_1	$2/3V_{dc}$	0
P	N	N	V_2	$4/3V_{dc}$	0

P	O	N	V_3	$2/\sqrt{3}^{-}V_{dc}$	$\pi/6$
P	P	O			
O	O	N	V_4	$2/3V_{dc}$	$\pi/3$
P	P	N	V_5	$4/3V_{dc}$	$\pi/3$
O	P	N	V_6	$2/\sqrt{3}^{-}V_{dc}$	$\pi/2$
O	P	O			
N	O	N	V_7	$2/3V_{dc}$	$2\pi/3$
N	P	N	V_8	$4/3V_{dc}$	$2\pi/3$
N	P	O	V_9	$2/\sqrt{3}^{-}V_{dc}$	$5\pi/6$
O	P	P			
N	O	O	V_{10}	$2/3V_{dc}$	Π
N	P	P	V_{11}	$4/3V_{dc}$	Π
N	O	P	V_{12}	$2/\sqrt{3}^{-}V_{dc}$	$-5\pi/6$
O	N	P			
N	N	O	V_{13}	$2/3V_{dc}$	$-2\pi/3$
N	N	P	V_{14}	$4/3V_{dc}$	$-2\pi/3$
O	N	P	V_{15}	$2/\sqrt{3}^{-}V_{dc}$	$-\pi/2$
P	O	P			
O	N	O	V_{16}	$2/3V_{dc}$	$-\pi/3$
P	N	P	V_{17}	$4/3V_{dc}$	$-\pi/3$
P	N	O	V_{18}	$2/\sqrt{3}^{-}V_{dc}$	$-\pi/6$

Conclusion

This chapter introduces the construction and principle of operation of induction motor, to be used for the analysis of the control method which is the direct torque control. A general classification of the control techniques for the IM methods have been introduced as well. three topologies of Voltage Source Multilevel Inverters have been presented with more explanation for the neutral point clamped inverter. In order to use the extension of classical DTC method a new space vector algorithm for three level-three phase inverter had been investigated.

Direct Torque Control

This chapter is devoted to investigate the principle operation for the DTC using the Control strategy based on three-level voltage inverter to facilitate the modeling of the DTC in VHDL code for the next chapter.

3.1 Introduction

In the past, electric drive speed regulations were realized using DC motors: for this kind of motors, the control was easy. However, their cost and maintenance were excessive. That is why, a recent solution which is called DTC (Direct Torque Control), has for control a three-phase asynchronous motor which is cheaper, and has high power/size ratio. The basic principles of the Direct Torque Control (DTC) method proposed by Takahashi and Noguchi in 1986 can be formulated as follows:

• Stator flux is a time integral of the stator EMF. Therefore, its magnitude strongly depends on the stator voltage.

• Developed torque is proportional to the sine of angle between the stator and rotor flux vectors.

• Reaction of rotor flux to changes in stator voltage is slower than that of the stator flux

3.2 **Direct flux-torque control fundamentals**

The DTC is principally a non-linear control in which the inverter switching states are imposed through a separate control of stator flux and electromagnetic torque of the motor. The inverter command is instantaneous and it replaces then the decoupling through the vector transformation.

One of the most important characteristics of the DTC is the non-linear regulation of stator flux and electromagnetic torque with variables structures or by hysteresis.

The flux regulation is imperative for an efficient control of the induction machine torque and in the DTC, the stator flux regulation is chosen because it is easier to estimate, and partly it has a faster dynamic than the rotor flux. By adjusting the stator flux, we also adjust the rotor flux. As in the other control methods, which use a direct regulation of the flux, the flux nominal value is imposed as a constant reference[17].

The general structure of the asynchronous motor with DTC using multilevel inverter is represented by the figure 3.1.

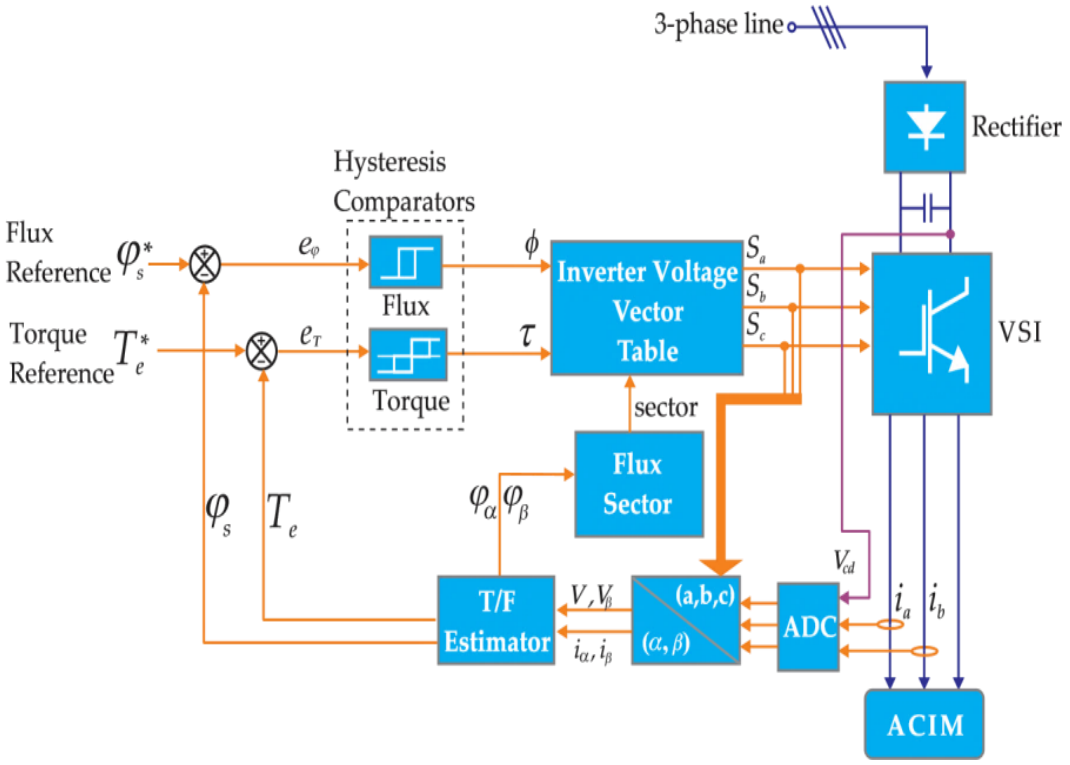

Figure 3.1 Direct torque control block diagram.

3.2.1 Stator flux control

The IM equations, in a stator reference frame, are defined from the previous equations (2.4.a), (2.4.b), (2.4.a) and (2.4.c).

The stator flux is estimated from the measure of stator current and voltage and their transformation in the $\alpha\beta$ subspace. So

$$\Psi_{s\alpha}=\int_0^t (U_{s\alpha} - I_{s\alpha}.Rs)dt \qquad \Psi_{s\beta}=\int_0^t (U_{s\beta} - I_{s\beta}.Rs)dt \tag{3.1}$$

The stator flux module and the linkage phase are given by:

$$\sqrt{\Psi_{s\alpha}{}^2 + \Psi_{s\beta}{}^2} = \Psi s \qquad \alpha_s=\tan^{-1}\frac{\Psi s\beta}{\Psi s\alpha} \tag{3.2}$$

On a sampling period Ts, and by neglecting the term ($Is.Rs$) in equation of stator flux, valid hypothesis for high speeds, the evolution of this last one is given by the vector Vs during Ts:

$$\Delta\Psi s = \Psi s - \Psi s_0 = Vs.Ts \quad (3.3)$$

Ψs_0 is the initial stator flux at the instant t_0 .

Ts: is the sampling time.

Vs: the voltage that will applied by the inverter.

So, the variation of the stator flux is directly proportional to the stator voltage, thus the control is carried out by varying the stator flux vector by selecting a suitable voltage vector with the inverter.

A two-level hysteresis comparator could be used for the control of the stator flux. So, we can easily control and maintain the flux vector Ψs in hysteresis bound as shown in figure3.2.

The value of the total bandwidth for the hysteresis loop is distributed symmetrically around the flux set point (reference) and dFlux is set to be HΨ.

.

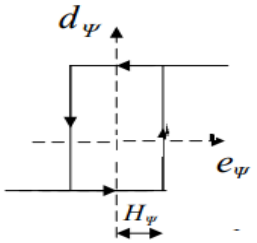

Figure 3.2 two-level hysteresis controller

The digitized output variable $d\Psi$ will have two values:

$d\Psi = 1$ for $e_\Psi > H\Psi$

$d\Psi = -1$ for $e_\Psi < -H\Psi$

where e_Ψ is the error computed from the deference of the reference flux and the measured one.

3.2.2 Torque control

The electromagnetic torque expression is defined as follows, where γ represents the angle between the rotor and stator flux vectors

$$Tem = 3/2.P\frac{Lm}{\sigma.Ls.Lr}|\Psi r|.|\Psi s|\sin\gamma \quad (3.5)$$

where P is the number of pole pair

L_m: mutual inductance

σ: leakage coefficient (Blondel coefficient) .

We deduct that the torque depends on the amplitude and the position of stator and rotor flux vectors.

On the other hand, the differential equation linking the stator flux and the rotor flux of motor is given by:

$$\frac{d\Psi r}{dt} + \left(\frac{1}{\sigma\tau r} - j\omega\right).\Psi r = \frac{Lm}{\sigma\tau r.Ls.}\Psi s \quad (3.6)$$

From this equation, the flux Ψ_r tracks the variations of the flux Ψ_s with a time constant $\sigma\tau r$*[18]* .

The expression of the electromagnetic torque is only obtained from the stator flux components $\Psi_{s\alpha}$, $\Psi_{s\beta}$ and currents $I_{s\alpha}$, $I_{s\beta}$:

$$Te=\frac{3}{2}P(\Psi_{s\alpha}i_{s\beta}-\Psi_{s\beta}i_{s\alpha}) \quad (3.7)$$

In controlling perfectly, the stator flux vector, from the vector *Vs*, in module and in position, we can control the amplitude and the relative position of the rotor flux vector and consequently the electromagnetic torque.

For the control of the electromagnetic torque, we can use a four-level hysteresis comparator which permits to have the two senses of motor rotation. The output of this corrector is represented by a digitized variable d_T indicating directly if the amplitude of the torque must be increased, decreased or maintained constant (d_T = -2, -1, 1, 2).

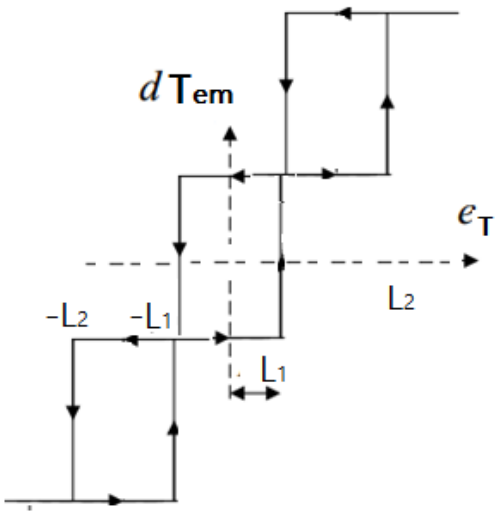

Figure 3.2torque four-level hysteresis controller

3.3 Control strategy of DTC based three-level voltage inverter

Three level inverter can be used in the command DTC, what allows to reduce advantage the harmonics, to have a high level of output voltage and can contribute to more reducing harmonics and the ripple torque. In that case, the space of voltages is subdivided into twelve sectors (instead of six with the classic DTC) and by considering the method of the virtual vectors, three sections with small, medium and large vectors can be exploited. We can also subdivide the space of voltages into only six sectors by adopting a technique which employs only twelve active voltage space vectors, corresponding to the small and large vectors and consequently without using the null or the medium space vectors and this is what we call **the natural extension of classical DTC**.

3.3.1 Flux Sector Identification

In order to re-orient the flux vector $\Psi_{s\alpha}$, first it is necessary to determine where it is localized. For this reason, the flux vector circular trajectory is divided into six symmetrical sectors, as shown in the figure3.3.

The angle α_s can be calculated, based on the α, β flux components as follows

$$\alpha_s = \tan^{-1}\frac{\Psi s\beta}{\Psi s\alpha} \tag{3.7}$$

However, implementing Eq.(3.7) in an FPGA is complex and time consuming and is usually performed be means of the coordinate rotation digital computer (CORDIC) algorithm [17]. Instead, it is possible to determine the sector in which the flux vector is located, based on the signs of the flux components. The sector can be determined by using Table 3.1 and Eq. (3.8).

$$\Psi_{ref} = \sqrt{3}|\Psi_\beta| - |\Psi_\alpha|. \tag{3.8}$$

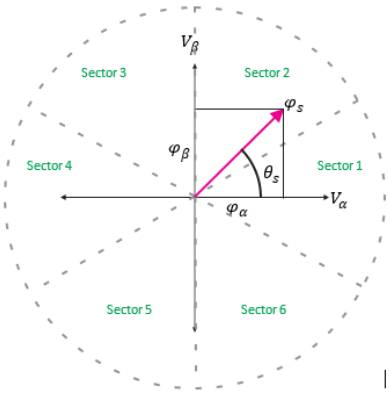

Figure 3.3Sectors of the flux vector circular trajectory.

Table 3.1 Stator flux space vector's sector.

Sing of $\Psi\alpha$	*Sing of Ψ_β*	*Ψ_{ref}*	*Sector N*
+	+/-	-	*1*
+	+	+	*2*
-	+	+	*3*
-	+/-	-	*4*
-	-	+	*5*
+	-	+	*6*

3.3.2 Switching table based on a natural extension of classical DTC

The elaboration of the command structure is based on the hysteresis controller output relating to the variable flux ($d\Psi$) and the variable torque (d_T) and the sector N corresponding to the stator flux vector position.

The command structure consists on a series of look-up tables, which contain for each sector the necessary voltage vector to apply at the multilevel inverter,

depending of the values returned by the hysteresis controllers. This control scheme, which uses only twelve active voltage space vectors corresponding to the sections with small and large vectors and without using the null and medium space vectors, is a natural extension of classical DTC for a two level inverter.

Table 3.2 Command structure look-up table

dΨ	d_τ	S_1	S_2	S_3	S_4	S_5	S_6
1	2	V_2^H	V_3^H	V_4^H	V_5^H	V_6^H	V_1^H
	1	V_2^L	V_3^L	V_4^L	V_5^L	V_6^L	V_1^L
	-1	V_6^L	V_1^L	V_2^L	V_3^L	V_4^L	V_5^L
	2	V_6^H	V_1^H	V_2^H	V_3^H	V_4^H	V_5^H
-1	2	V_3^H	V_4^H	V_5^H	V_6^H	V_1^H	V_2^H
	1	V_3^L	V_4^L	V_5^L	V_6^L	V_1^L	V_2^L
	-1	V_5^L	V_6^L	V_1^L	V_2^L	V_3^L	V_4^L
	2	V_5^H	V_6^H	V_1^H	V_2^H	V_3^H	V_4^H

Further analysis on table 3.2 reveals that the output as one of the following structures, V_x^L or V_x^H, where letters “L” and “H” stand for low and high, respectively. And as shown by the figure 2.10 the high vectors $V_1^{H,}$ V_2^H, V_3^H, V_4^H, V_5^H and V_6^H are represented respectively by the configuration states of the inverter (PPN), (PPN), (NPN), (NNP), (NPP), (PNP). And for the low vectors $V_1^{L,}$ V_2^L, V_3^L, V_4^L, V_5^L and V_6^L are represented respectively also (ONN), (OON), (NON), (NOO), (NNO), (ONO).

the following figure shows the selected voltage vector for each sector to maintain the stator flux in the hysteresis bound

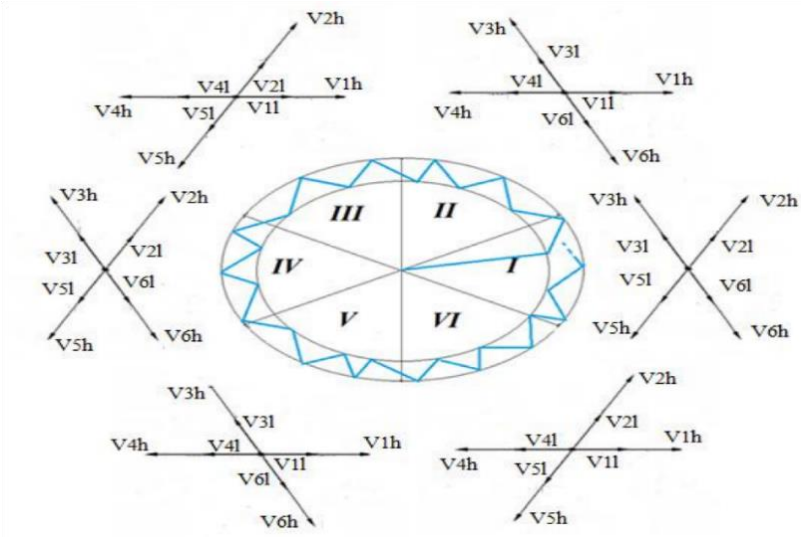

Figure 3.4 – DTC available voltage vectors

3.4 **conclusion**

In this chapter, The Direct flux-torque control fundamentals discussed begin with controlling the stator flux and therefore, the control the torque is possible, using Switching table based on three-level voltage inverter to apply the natural extension of classical DTC method**.**

4

Implementation and Results

Based on the background theory presented in previous chapters, in this chapter, the hardware and software implementation of Direct Torque Control for induction motors is introduced. In software part FPGA implementation of DTC algorithm using VHDL blocks is shown. The three levels inverter implementation using PCB presented as hardware part. Then results of this thesis to be discussed at the end of the chapter.

4.1 Software Implementation

4.1.1 The Architecture of DTC Implementation

All the equations modeling the behavior of motor are implemented in a three-stage-pipelined architecture, as in Fig4.1. Several mathematical operations are performed in parallel. At the first stage, stator currents and voltages in αβ-coordinates are calculated in parallel, so that those results can be used to estimate the stator flux at the same stage. The resulted currents and flux are used to determine the flux magnitude and the torque estimation in the second stage. Then Compared with flux and torque reference values. the results go through hysteresis controllers to lookup table generating the set of inverter switches[19].

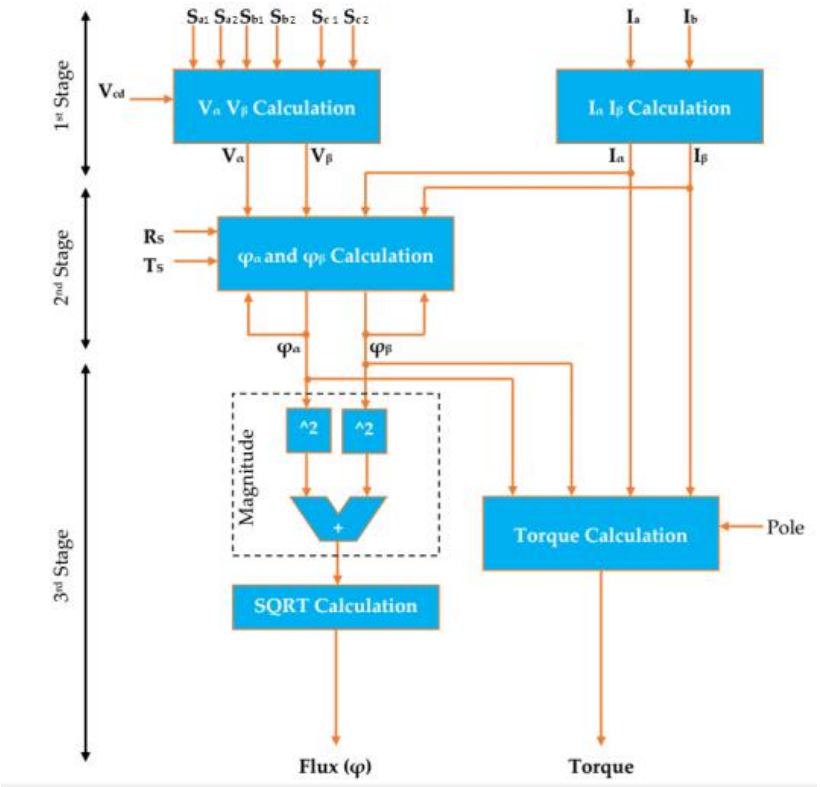

Figure 4.1 The architecture of flux and torque estimation

4.1.2 The Digital Properties of DTC Algorithm

To achieve a good implementation, several digital properties need to be considered when designing these estimators. Adopted binary format, quantization and sampling time are amongst the key factors.

4.1.2.1 Binary Format Representation

In this implementation, two's complement fixed-point representation is used during all the operations, except for the square root calculation. In this particular case, unsigned fixed-point representation is applied, since its operand and its results are always positive.

4.1.2.2 Quantization

The determination of word size (word length) is one of the critical parts in FPGA implementation. On one hand, the use of an insufficient number of bits may reduce the precision or cause a calculation error, which can destabilize the whole system. On the other hand, the use of larger words may increase the hardware implementation area.

4.1.2.3 Sampling time

The sampling time T_s is set to be 5 μs due to the hardware limitation. Therefore, all the operations involved in this model are performed within this sampling time.

4.1.3 The VHDL Design of DTC

The DTC model is implemented on FPGA with VHDL architecture consisting of ten main blocks. The VHDL codes were simulated in ModelSim before being synthesized and implemented on FPGA.

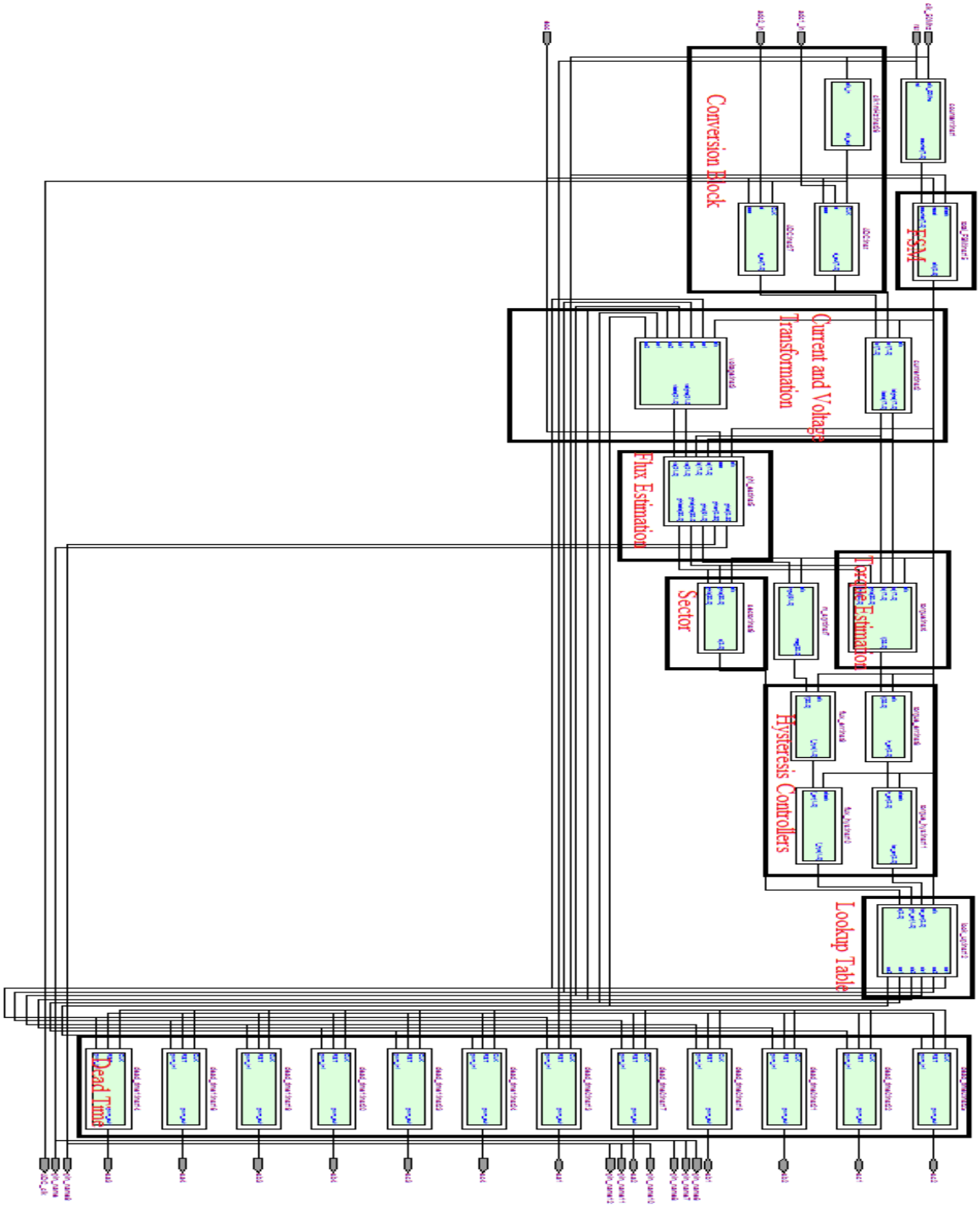

Figure 4.2: RTL view of DTC

4.1.3.1 Conversion Control Block

The current signals (I_a, I_b) are first obtained by sensing two of the motor lines by means of coil sensors. The output is an AC signal that is amplified and added a DC offset, in order to have a positive only value between 0 and 4 V for the ADC. The signals are then converted by MC145040P1 ADC to a serial 8-bit value and then to a 8-bit parallel value. Finally, the offset value is subtracted and multiplied by a scaling factor in order to obtain the original current signal.

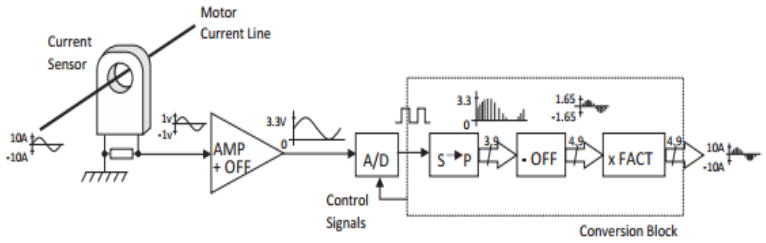

Figure 4.3Current signal conversion process from current sensor to conversion control block

4.1.3.2 I_α and I_β Calculation

The function of this block is to transform the stator phase currents I_a, I_b and I_c into the stationary α-β coordinates (I_α and I_β) refer to the equations

$$I_\alpha = I_a \qquad (4.1)$$

$$I_\beta = \frac{\sqrt{3}}{3}(I_a - 2I_b) \qquad (4.2)$$

In this design, the values (I_a,I_b) and (I_α and I_β) are represented on 17-bits and 18-bits two's Complement fixed-point form at [5.12 bit] and [6.12 b it] respectively to get the precise values. to avoid overflow that the result calculation of "I_a+2I_b" and $\frac{\sqrt{3}}{3}$ of the current equation are represented each on 19 bits, as [7.12] and [1.18] .

The output of the signed multiplier is represented on 38-bits, as [8.30]. However, the I_β is only represented on 18-bits as [6.12] to minimize hardware resource, so the 38-bit [8.30] is truncated to become 18-b it [6 .12]. Based on the evaluation result, the 18-bit has been considered suitable to represent I_β precisely.

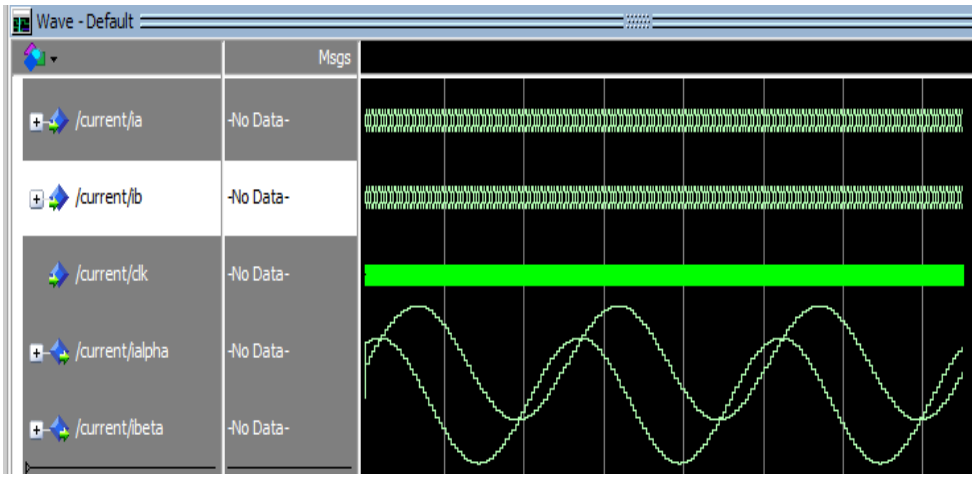

Figure 4.4ModelSim verification of current transformation block

4.1.3.3 V_α and V_β Calculation:

The function of this block is to calculate the stator voltages in α-β components refer to the equations

$$V_\alpha = \frac{V_{dc}}{3}\left(2(s_{a1} + s_{a2}) + (s_{a1} + s_{b2}) + (s_{c1} + s_{c2})\right) \quad (4.3)$$

$$V_\beta = \frac{\sqrt{3}V_{dc}}{3}\left((s_{a1} + s_{b2}) - (s_{c1} + s_{c2})\right) \quad (4.4)$$

The input is 12-bit high voltage DC-supply and six switching status. The output voltages are represented in 22-bit two's-complement fixed-point format [10.12]. The RTL viewer of the calculation is shown in Fig4.5.

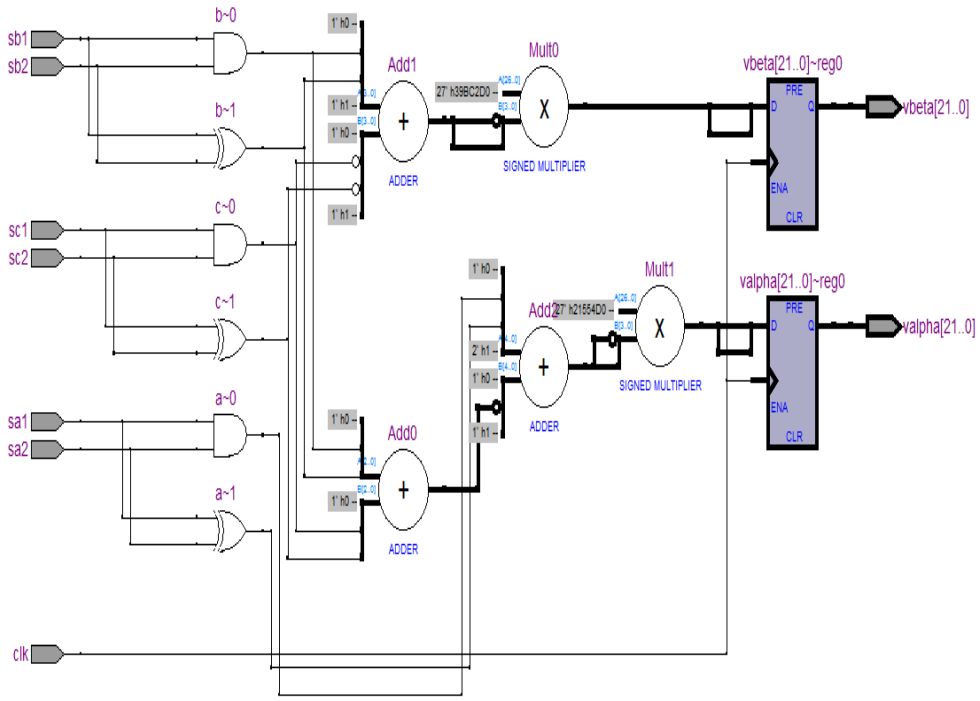

Figure 4.5 RTL view of Voltage Transformation Block

The numbers 27' h39B6C2D0" and "19' h21554D0" are to represent $\frac{\sqrt{3}}{3}$ and $\frac{1}{3}$ in voltage equation It is important to note that the results (before truncated) of the V_α and V_β are allocated each to 34-bit, as [16.18], but the final values of the V_α and V_β are only 22-bit. The most significant 9-bit and least significant 6 -bit of each the Vα and V_β 34-bits are truncated, so only $27^{th} - 6^{th}$ bits are used to represent the final values of each the V_α and V_β as 22-bit, i.e. [10.12]. The truncations are conducted to minimize hardware resources, while still retaining sufficient precision.

4.1.3.4 φ_s Calculation

4.1.3.4.1 φ_α and φ_β Calculation

After the calculation of α-β components of current and voltage, the α-β flux is calculated in this block The other input, R_s, is represented on 10-bits (5. 5 bit). The

output α-β components of the stator flux are represented in 31-b it two's-complement fixed-point format [4.27]. In this paper, the sampling time (T_s) is5 µs. The value of T_s is represented in [1.27]. Consider the ($1-\omega_c*T_s$) filter, the part is selected: 0.999975. In this case, the value is represented in [1.22] as "23' h3FFF97"(=4194199), so 0.999974966 will be obtained to represent the 0.999975 filter. The filter is designed to overcome the problem of integration drift. Therefore, the low-pass filter is used to replace the pure integrator with appropriate cut-off frequency (5 rad/s).

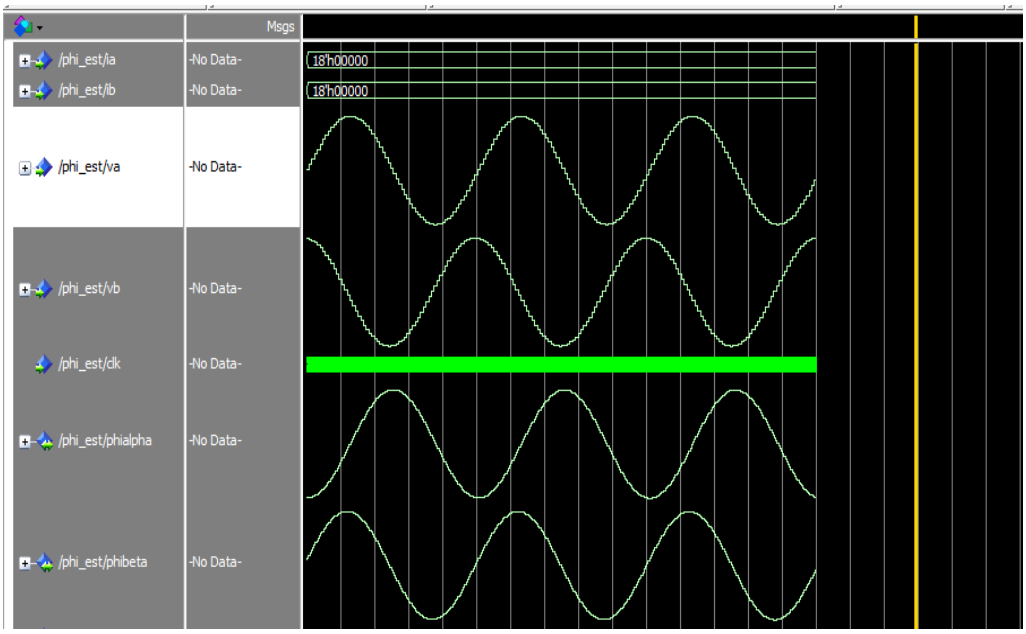

Figure 4.6 ModelSim Verification of Flux Estimation Block

4.1.3.4.2 Magnitude Calculation

This block is designed to calculate the magnitude of the stator flux. The inputs of the block are the α-β components of stator flux, and the output is their magnitude, which is represented in 62bits fixed-point format (8.54 bit).

4.1.3.4.3 Square Root Calculation

This block is designed to calculate stator flux φ_s using modified non-restoring square root algorithm. The first output of the block is represented in 31 bit fixed- point format, and the n it is truncated to 17 bit. The principle of the principle of calculation is based on powerful improved method presented in reference[20].

4.1.3.5 Determination of Sector

The work has introduced a simple method to determine the sector of flux vector, based on comparison between φ_α , $\sqrt{3}\varphi_\beta$,$-\sqrt{3}\ \varphi_\beta$ and 0. which is modified from [21]. With the comparison, it is simpler to determine the sector of the voltage vector, compared to the conventional methods of using arctangent. as shown in Table 4.1.

Table 4.1Karnaugh Map of The Proposed Simpler Identification of Sector

The input			The output (Sector)	
$\varphi_\alpha > 0$	$\varphi_\alpha > \sqrt{3}\varphi_\beta$	$\varphi_\alpha > -\sqrt{3}\ \varphi_\beta$	In binary	In decimal
0	0	0	100	4
0	0	1	011	3
0	1	0	101	5
0	1	1	Xxx	xxx
1	0	0	Xxx	xxx
1	0	1	010	2
1	1	0	110	6
1	1	1	001	1

Karnaugh map of the proposed sector identification. Through the simplification, it will be possible to get simpler logic of the sector analysis for FPGA implementation through VHDL gate level coding; each sector is represented on 3-bits.

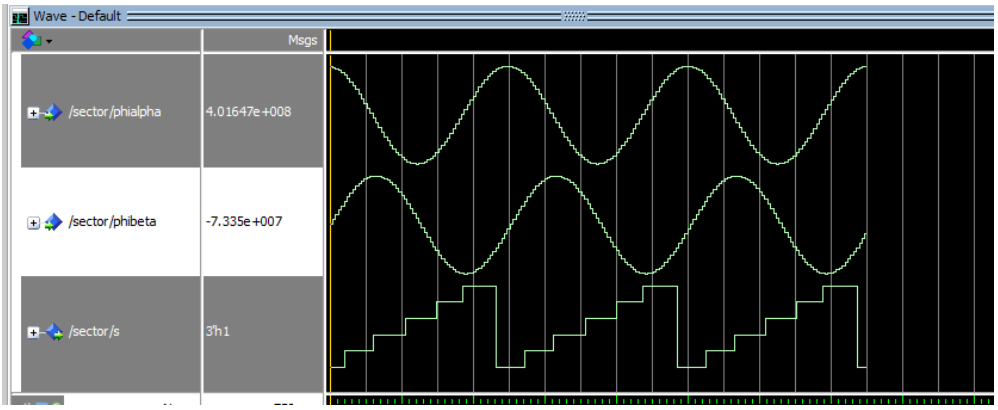

Figure 4.7 ModelSim verification Sector Identification Block

4.1.3.6 Torque Calculation

The function of this block is to calculate the torque as given in equation (2.6). the output is represented in 55 bits [14.41] fixed point format and then it truncated to 26 bits [6.20].

4.1.3.7 Reference Comparison Block

In this DTC block, the estimated flux and torque values are subtracted from the corresponding reference values. The structure of the comparison block is shown in Figure4.8.

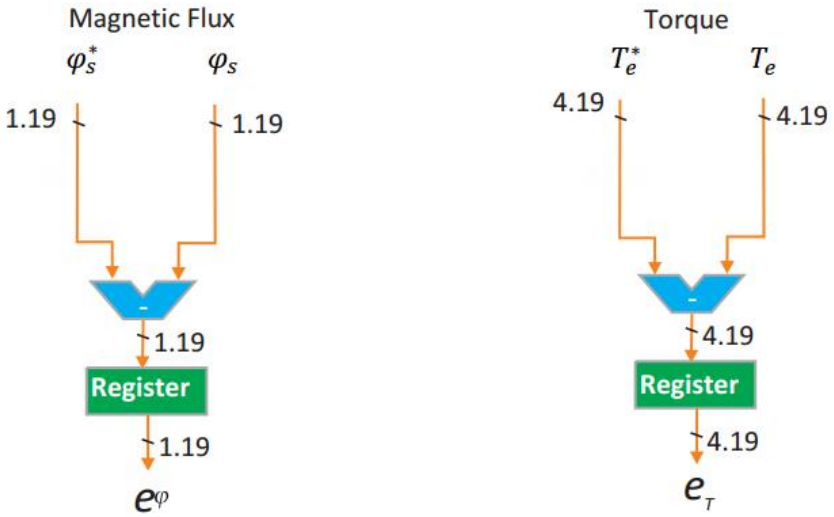

Figure 4.8 reference compression of flux and torque

4.1.3.8 Hysteresis Comparators

Both the stator flux and torque controllers are responsible to generate the appropriate error status of the stator flux and torque. A two-level comparator for flux with band error [$-L_\varphi$, L_φ] and a four-level comparator for torque are implemented in this block with error band [$-L_2$, $-L_1$], [$-L_1$, L_1] and [L_1 , L_2]. Both hysteresis comparators were designed as FSMs in order to provide fast transition from one to another state. The FSM for the hysteresis comparators are shown in Figures4.9 and Figures4.10 .

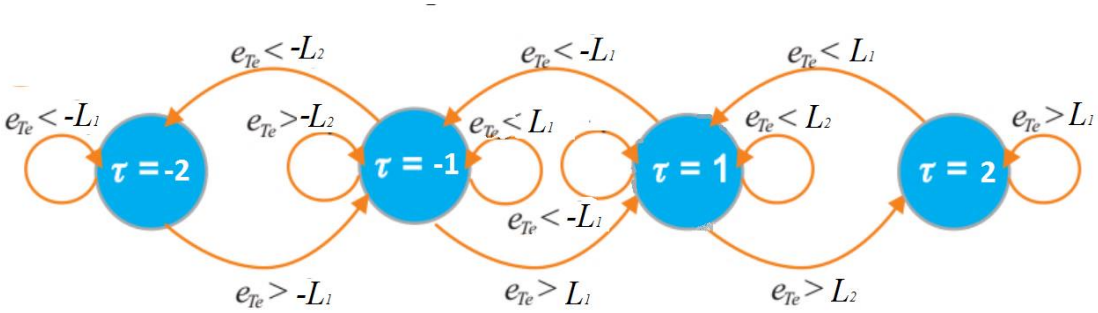

Figure 4.9 FSM for torque hysteresis controller

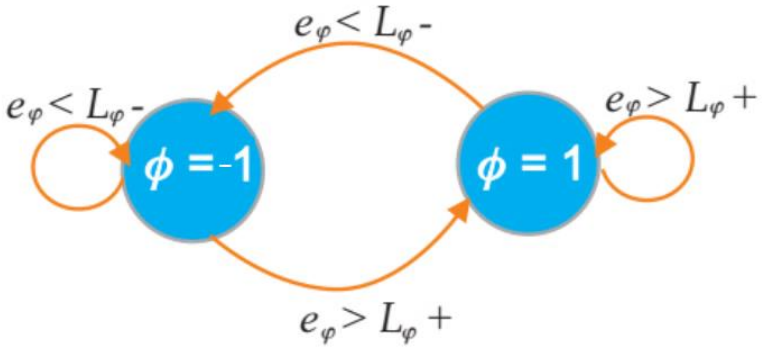

Figure 4.10 FSM for Flux Hysteresis Controller

4.1.3.9 Switching Table

The VSI optimal switching vectors listed in Table (2.2) are included in the switching table. A voltage vector is selected based on the hysteresis comparator values ϕ and τ, and on the flux vector sector. The table output is a 6-bit vector and its complement, which are fed to the VSI. The 6-bit vector is also sent back to the torque-flux estimator to obtain the next torque and flux values.

4.1.3.10 Dead Time

Dead time is created to complementary PWM signals (one on when the other off) to avoid any short circuit occurrence. The VHDL code take the switches state and creates 1 us dead time between complementary switches. co-simulation results shown in Figure 4.11.

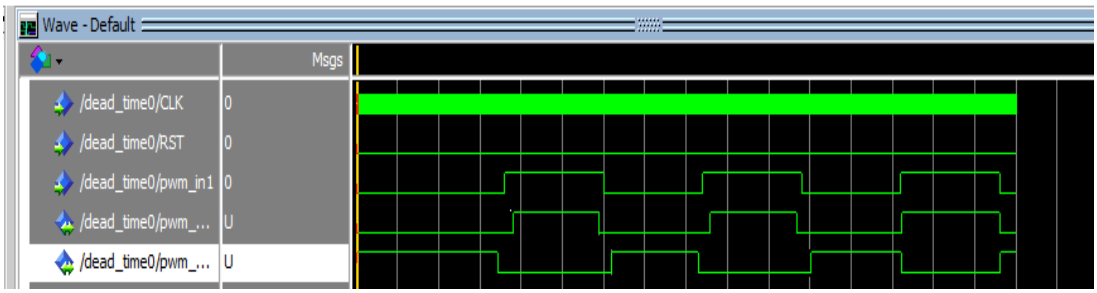

Figure 4.11 ModelSim Co-simulation of Dead Time Block

4.1.3.11 Synchronizations:

A finite state machine (FSM) is included in this block and is in charge of the control of all the other DTC blocks. In order to have a constant sampling period (T_s), a global FSM was used the data flow from one block to the next. Since there is a register at the output of every major block, the FSM sends a timed pulse to each one, depending on the selected width of the data path. The synchronizations are designed in one cycle of the sampling time (in this case 5 µs).

4.2 **Hardware Implementation**

In this section the three level NPC inverter discussed in chapter 2 and from the schematic diagram in figure 4.12, The circuit will be implemented on printed circuit board PCB to achieve the desired output voltage that is needed to maintain the torque and the flux at some reference values using the generated pulses from the FPGA to gate the driving circuitry that is responsible to turn off and on the MOSFETs, and then ending up by the power circuitry that will be responsible for generating the power signals for the induction motor as shown in figure 4.13.

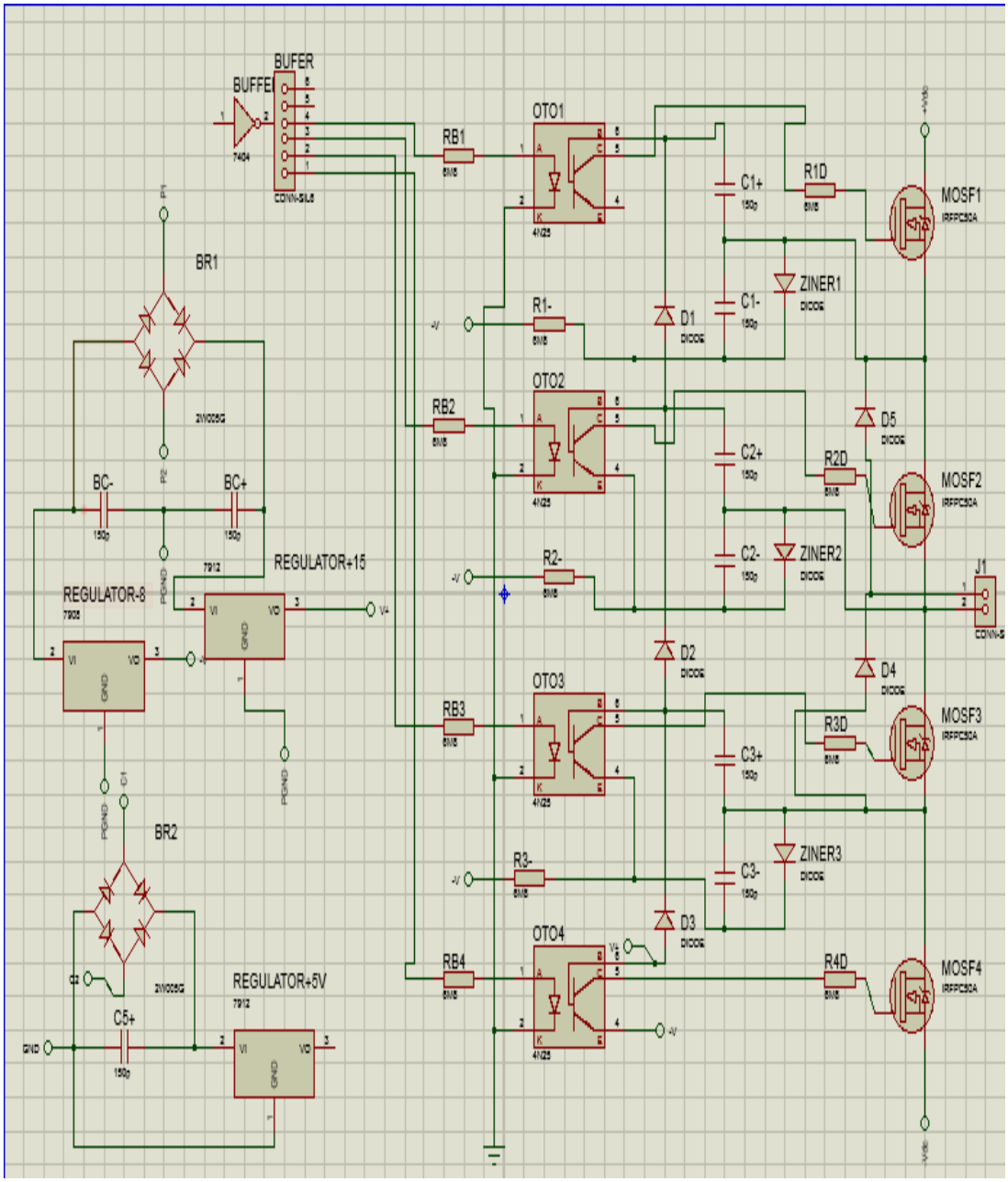

Figure 4.12 Schematic Diagram of three level inverter one phase

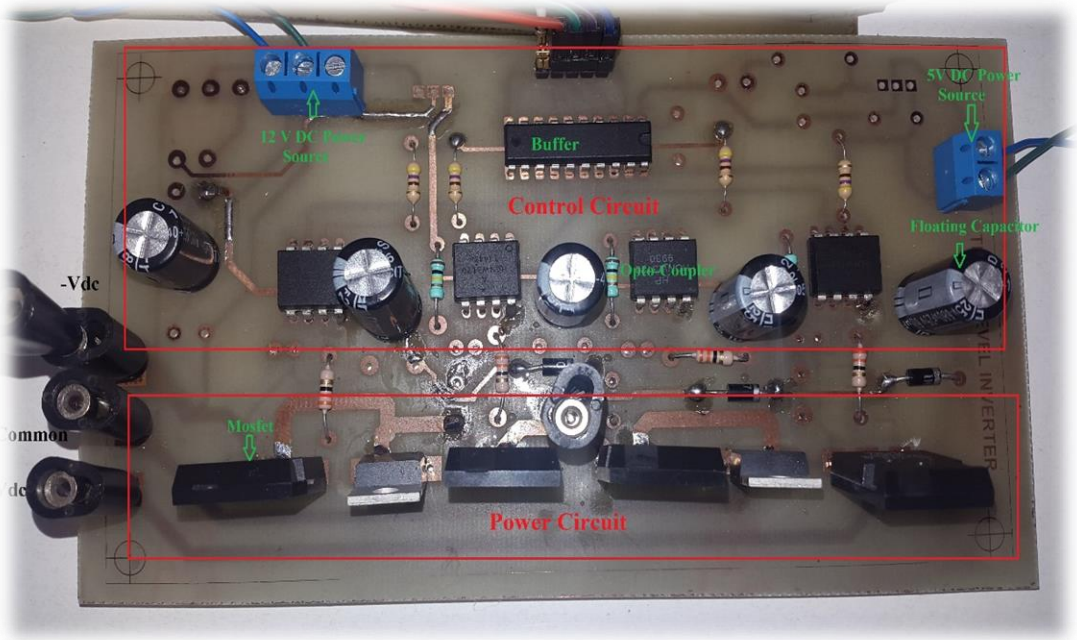

(a)

(b)

Figure 4.13 (a)Three Level inveter one phase

(b)Three Level inveter three phase

As it is shown in the figure 4.13 (a) the three level inverter leg consist of two main circuits.

4.2.1 control circuit

The control circuit is responsible to control the switching on and off MOSFETs. It consists of different components:

- "4LS540 MOTOROLA" buffer: its main role to protect the FPGA from high current,
- "HCNW3120AVAGO technologies" optocoupler: four identical optocouplers are used as opto-isolators. The optocoupler transfers electrical signals between two isolated circuits using light to protect the control circuit from the high voltages.
- Three identical diodes to implement the floating power supply with different resistors with variety of values.
- DC sources with Two power supplies are used in order to feed the electronic components within the circuit, one 5 V was used to feed the buffer and 12 volts for the optocouplers.

To minimizing the 12 DC sources used to power the optocouplers. A one DC source the Bootstrap Supply method is used, which is a common technique employed to generate a floating supply, the bootstrap supply is a simple circuit using only one diode and a supply storage capacitor.

In our configuration four capacitors, one power supply used in lowermost optocoupler where the voltage is pumped to the other optocouplers through the charging of the other capacitors, this way enabling this IC's to deliver the switching signals to the different gates of the power valves through a small resistor.

4.2.2 Power circuit

For the power circuit three main components used to have the output voltages are:

- **Power diodes:** The two are used referenced by BY329 Philips, these clamping diodes responsible for clamping and blocking the voltage between the capacitors and switching devices, these two diodes are connected to the neutral
- **Power MOSFET:** A MOSET is a type of transistor used for switching. Four MOSFET with the reference of (BUK555/100A -Philips Semiconductors-) are used in our circuit in which the turning on/off of this MOSFETS allow us to generate voltage levels though the proper switching of them within each leg.
- **Power supplies**: Since we were only doing testing in our laboratory the power supply is used as input power for the inverter instead of two charged polarizing capacitor, and for avoiding the unbalance voltage for each capacitor as well.

4.3 Results and Discussion

In this section, The DTC simulation and implementation results presented and studied for different operating conditions. Ending up with a discussion of obtained results.

4.3.1 Experimental results

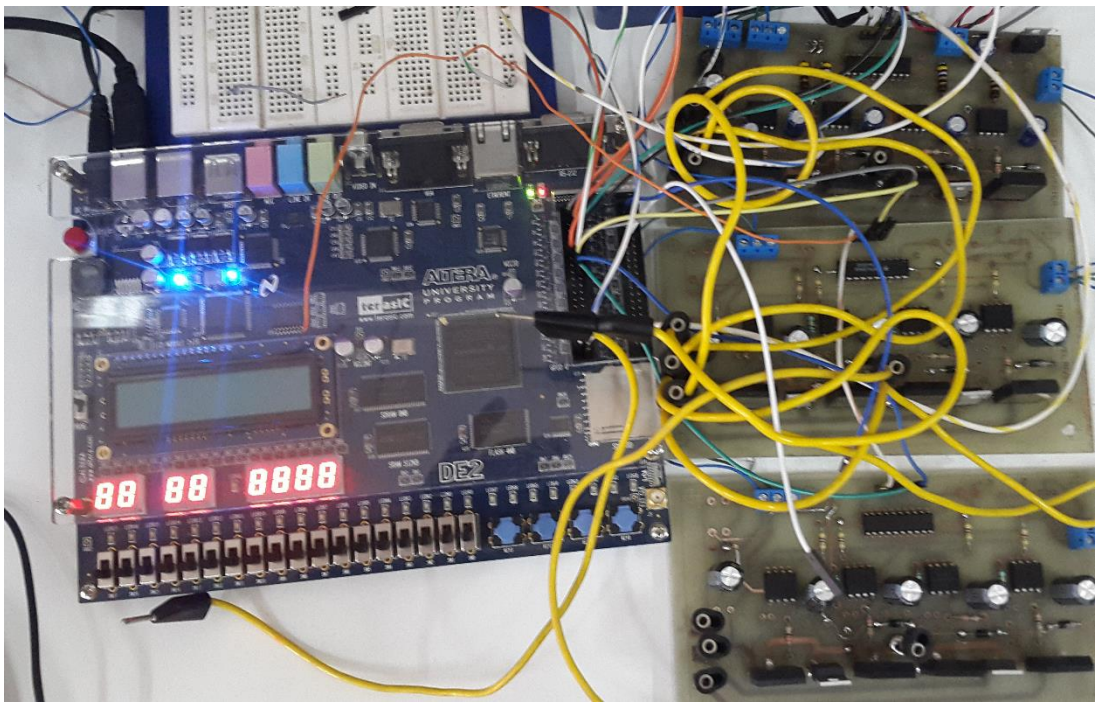

Figure 4.14 DTC implementation using FPGA with three level inverter

For experimental verification, the DTC strategy was implemented on a DE2 board FPGA running at 50 MHz.

The objective of this test is to observe the capability of the control model stability and response time compared to a fixed flux reference with zero input current (without motor current).

After loading DTC algorithm on FPGA the output switches for one inverter leg are checked as shown in figure 4.13.

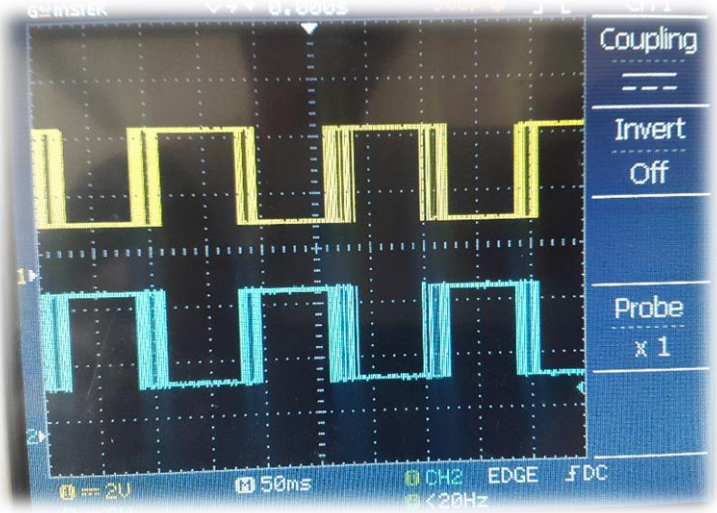

Figure 4.15 The switching signals (PWM pulses) for leg 1

The results obtained from the previous figure show the switching state for switch s_{a1} and $s_{a3,}$ and the same for the other switches.

To avoid the short circuit on one leg for the inverter the complementary switch should have a dead time to be on or off. As explained in section 4.1.3.10 the dead time is 1us.this can be seen on the figure 4.15.

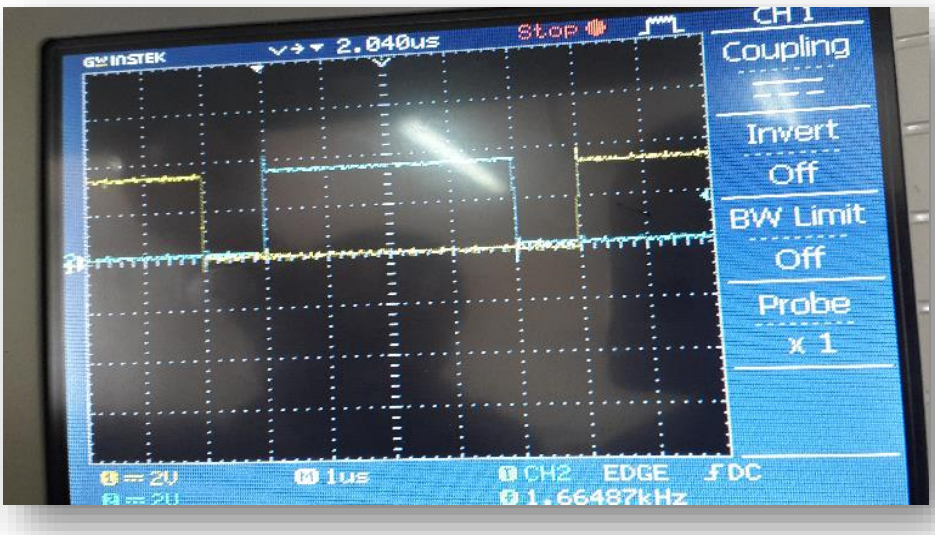

Figure 4.16 Dead Time For Sa1 and Sa3

The output switches go to drive the three-level inverter to generate the output voltage of induction motor, figure 4.16 shows phase to phase voltage.

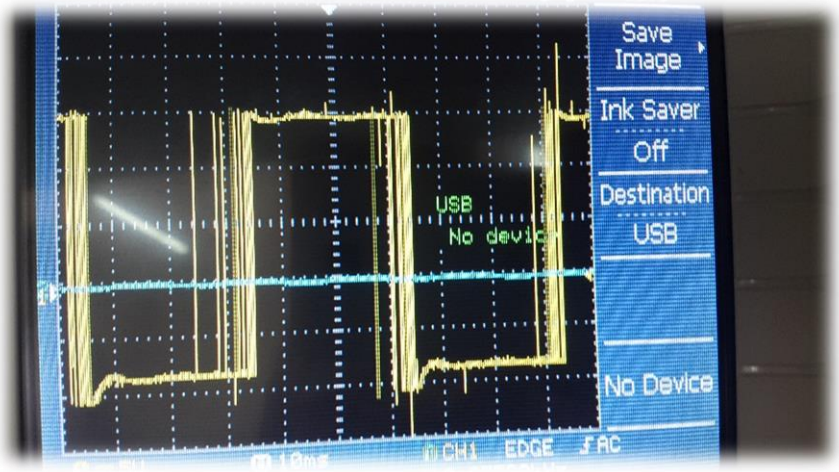

Figure 4.13Phase to phase output voltage

Because of the property of the two level inverter used in DTC algorithm the output voltage is will vary between $+V_{dc}$ and $-V_{dc}$.

To visualize the FPGA flux locus on the oscilloscope, two 8-bit digital to analog converters(DAC0801) were used. The resulting flux with 0.5 Wb magnitude is shown in Figure.

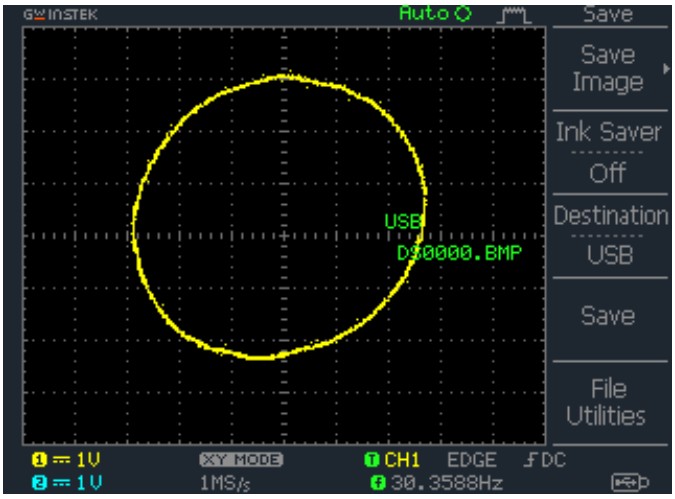

Figure 4.18 The Flux Locus Result(0.2Wb/div)

due to the small sampling time, it is possible to reduce the flux hysteresis band to a very small value the locus of the flux is almost a perfect circle, with very small ripple. Consequently, one will expect almost a sinusoidal stator flux.

4.4 **Discussion**

The DTC algorithm was designed based on a structural description and generic VHDL blocks, to make the control easily re-scalable and completely independent of the FPGA technology.

Two´s complement fixed-point format and variable word size for all arithmetic calculations is simplest and most effective technique, to achieve a good implementation DTC, and consumes minimum hardware resource usage.

The synchronization is designed in one cycle of the sampling time this can be achieved easily by using finite state machine.

MATLAB/Simulink and Modelsim Co-Simulation gives an effective way to evaluate the correctness and validate each VHDL block of the proposed DTC.

The results of DTC algorithm test shows a perfect response of the control model to reference flux value, with a small hysteresis ripples. Due to the low sampling period (high sampling frequency).

In other words, the hysteresis ripple in flux can be minimized by employing a faster sampling time. The 5 μs sampling time (in the flux and torque estimators) can only be achieved by employing FPGA. With the DSPs and microprocessors available in the market today, it may not be possible to implement such high sampling frequency.

4.5 **Conclusion**

As conclusion the natural extension of classical DTC algorithm has been successfully implemented on the FPGA to control the induction motor to get the desired flux and torque references. Therefore, the resulting of the flux was perfect equally to the reference value.

5

General Conclusion

5.1 Conclusion

In this thesis the natural extension DTC principle is presented and it is shown that with a simple algorithm using look- up table for a three-level inverter based on a standard two-level inverter we can implement this method easily using Field Programmable Gate Arrays (FPGA) with VHDL code. The DTC performance is significantly improved by the use of FPGA, which can execute the DTC algorithm at higher sampling frequency with parallel execution, this leads to the reduction of the torque ripple and improved flux and torque estimations.

The main achievements in our implementation were in calculating a discrete integration operation of stator flux with modifying a non-restoring method in calculating the complicated square root operation in stator flux estimator, increasing the sampling frequency to 200kHz such that the digital computation will perform similar to that of the analog operation, and using the two's complement fixed-point format approach to minimize calculation errors and the hardware resource usage in all operations. The design was achieved in VHDL, based on ModelSim to validate each block for the whole system.

5.2 Drawbacks:

Despite in fact that, the DTC is one of the robust techniques to control the torque and the flux, still has some disadvantages.

- DTC has the high torque and stator flux linkage ripples. Since the switching state of inverter is updated once every sampling time, the inverter keeps the same state until outputs of each hysteresis controller changes states.
- Stator flux estimation is achieved by integrating the difference between the input voltage and the voltage drop across the stator resistance.
- The stator flux linkage estimation has stator resistance, So any variation in the stator resistance introduces error in the stator flux linkage computation.

5.3 Future Work

Although this dissertation has covered many issues and challenges of DTC additional work has been left for the future, some of those possible works are listed below:

- Complete the second goal to achieve the desired output torque.
- Applying 24 active vectors with 12 twelve sectors for the three level inverter to achieve more precise results.
- Instead of using the hysteresis controller, the PI controllers and a space vector modulator (SVM) used.

References

[1]. Takahashi and T. Noguchi. A New Quick-Response and High-Efficiency Control Strategy of an Induction Motor. IEEE Transactions on Industry Applications. 1986; IA-22(5): 820-827.

[2] A. Jidin, et al., "Torque ripple minimization in DTC induction motor drive using constant frequency torque controller," in Electrical Machines and Systems (ICEMS), 2010 International Conference on, 2010, pp. 919-924.

[3] D. Casadei, G. Serra, A. Tani, "Constant frequency operation of a DTC induction motor
drive for electric vehicle", Proc. of ICEM Conf., Vol. 3, 1996, pp. 224-229

[4] Bahri I., Idkhajine L., Monmasson E., El Amine Benkhelifa M. Hardware/Software Codesign Guidelines for System on Chip FPGA-Based Sensorless AC Drive Applications. IEEE Transactions on Industrial Informatics. 2013; 9(4):2165-2176. DOI: 10.1109/ TII.2013.2245908

[5] Amol A. Kalage, M.Vasant,"Modeling and Simulation of FPGA based direct Torque Control of Induction Motor Drive", International Journal of Recent Trends in Engineering, vol.1, no.4, May 2009.

[6] www.automatedbuildings.com [Online], accessed on May 19th, 2015. Available on: http://www.automatedbuildings.com/news/jul01/art/abbd/abbd.htm

[7] Austin Hughes. Electric Motors and Drives Fundamentals, Types and Applications. 3rd ed. Newnes, 2006

[8] Lepka J., Stekl P. 3-Phase AC Induction Motor Vector Control Using 56F80x, 56F8100 or 56F8300 Device. Freescale Application Note. 2005; 1-68.

[9] Holtz, J. 1995. "The Representation of AC Machine Dynamics by Complex Signal Flow Graphs", in IEEE Trans. Ind. Appl., Vol. 42, No. 3, pp. 263-271

[10] Guzinski, J et al.,Sensorless induction motor drive for electric vehicle application, International Journal of Engineering, Science and Technoology, 2010 pp.20-34

[11] Adam, Ali A., Gulez, Kayhan, Torque control of PMSM and associated harmonic ripples,Fatih Einversity, Electrical-Electronics Eng. Dept.

[12] D. Casadei, F. Profumo, G. Serra, A. Tani, "FOC and DTC: two viable schemes for induction motors torque control", IEEE Transactions on Power Electronics, Vol. 17,Issue: 5, Sept. 2002,pp.779-787.

[13] Rodriguez,J. et al, Multilevel Voltage Source Converter Topologies for Industrial Medium Voltage Drives, IEEE Transactions on Industrial Electronics, Vol.54, 2007

[14] S. Bum-Seok, G. Sinha, M. D. Manjrekar, and T. A. Lipo, "Multilevel Power Conversion;An Overview Of Topologies And Modulation Strategies," in Optimization of Electrical and Electronic Equipments, 1998. OPTIM '98. Proceedings of the 6thInternational Conference on, 1998, pp. AD-11-AD-24.

[15] A,Nabae,I.Takahasai and H. Akagi, "A new neutral-point-clamped PWM inverter," IEEE Transactions in Industry Applications, vol. IA – 17, no 5, pp. 518 – 523, Sept./Oct. 1981.

[16] A, Nabae, I. Takahasai and H. Akagi, "A new neutral-point-clamped PWM inverter," IEEE Transactions in Industry Applications, vol. IA – 17, no 5, pp. 518 – 523, Sept./Oct. 1981.

[17] Lis J., Kowalski C.T., Orlowska-Kowalska T. Sensorless DTC Control of the Induction Motor Using FPGA. IEEE International Symposium on Industrial Electronics; June 30th; Cambridge: IEEE; 2008. p. 1914-1919. DOI: 10.1109/ISIE.2008.4677287

[18] Direct Torque control based multi-level inverter and artificial intelligence techniques of induction machine (DFI G), LAMCHICH Moulay Tahar, LACHGUER Nora University Cadi Ayyad/ Faculty of Sciences Semlalia/Department of Physic/Laboratory of Electronic and Instrumentation Morocco.

[19] S. Ferreira, *et al.*, "Design and prototyping of direct torque control of induction motors in FPGAs," in *Integrated Circuits and Systems Design, 2003. SBCCI 2003. Proceedings. 16th Symposium on*, 2003, pp. 105-110.

[20] T. Sutikno*, et al,."a simple strategy to solve complicated square root problem in DTC for FPGA implementation" In industrial Electronics & application (ISIEA),2010 IEEE Symposium on 2010. pp 691_695.*

[21] T. Sutikno*, et al,."New approach FPGA based implementation of discontinuous SVPWM ",turk J ELEC Eng & Comp Sci*. vol. 18, p 6,2010.